Title

Extended voltage imaging in cardiomyocytes with a triplet state quencher-stabilized silicon rhodamine

Authors

Kayli N. Martinez,[1†] Nels C. Gerstner,[1†] Samantha Yang,[1] and Evan W. Miller*[1,2,3]

Affiliations

[1]Department of Chemistry, [2]Department of Molecular & Cell Biology, and [3]Helen Wills Neuroscience Institute

University of California, Berkeley. Berkeley, CA. 94720-1460.

*evanwmiller@berkeley.edu

[†]equal contribution

Abstract

Voltage imaging of cardiac electrophysiology with voltage-sensitive dyes has long been a powerful complement to traditional methods like patch-clamp electrophysiology. Chemically synthesized voltage sensitive fluorophores offer flexibility for imaging in sensitive samples like human induced pluripotent stem cell derived cardiomyocytes (hiPSC-CMs), since they do not require genetic transformation of the sample. One serious concern for any fluorescent voltage indicator, whether chemically synthesized or genetically encoded, is phototoxicity. We have been exploring self-healing fluorophores that use triplet state quenchers (TSQs) as a means to reduce the already low phototoxicity of VoltageFluor dyes developed in our lab. We previously showed that conjugation of the TSQ cyclooctatetraene (COT) to a fluorescein based VoltageFluor dye substantially reduced phototoxicity. Here, we show that this approach can be applied to far-red Silicon rhodamine dyes. COT-conjugated Si-rhodamines show improved photostability and reduced phototoxicity in hiPSC-CMs compared to the unmodified dye. This enables imaging of hiPSC-CMs for up to 30 minutes with continuous illumination. We show that this effect is mediated by a combination of reduced singlet oxygen production and lower loading in the cellular membrane. We discuss future applications and avenues of improvement for TSQ-stabilized VoltageFluor dyes.

Introduction

Voltage sensitive fluorescent indicators have long been used for the direct visualization of cardiac electrophysiology. These indicators complement traditional methods of monitoring cardiac electrophysiology such as whole-cell patch clamp electrophysiology.[1] The use of patch clamp electrophysiology has helped determine the electrophysiological effects of structural immaturity in hiPSC-CMs and provided insight into action potential (AP) parameters.[2] However, the patch clamp technique is difficult, lacks spatial resolution, is low throughput, and is often terminal.[1] Voltage sensitive indicators offer a complementary method for studying electrophysiology and have led to progress in whole-heart optical mapping and understanding of cardiac arrhythmias.[3,4] More recently, fluorescent indicators have been used in the characterization of human induced pluripotent stem cell-derived cardiomyocytes (hiPSC-CMs),[5–8] as well as in screening assays for arrhythmias and drug toxicity, including screening for COVID- therapeutics.[9–12]

Fluorescence imaging of cardiac electrophysiology dates to 1976 with the study of frog hearts with merocyanine 540.[13] Since that time, toxicity and phototoxicity of voltage-sensitive dyes has been a primary concern, along with photobleaching.[14–18] While phototoxicity and photobleaching can be reduced by altering experimental parameters such as light intensity and exposure times,[19–21] this comes at a steep cost of decreased sensitivity and signal-to-noise. There is therefore a need for the design of new, less toxic voltage sensitive indicators.[2,22]

VoltageFluors (VFs) are a class of voltage sensitive indicators that we hypothesize utilize a photoinduced electron transfer (PeT) mechanism to sense changes in membrane potential.[23–25] VF dyes possess fast, linear, and turn-on optical response to membrane potential depolarizations.[26] The low phototoxicity of VF2.1.Cl can be further reduced by modifications to the molecular wire.[27,28] We sought a more generalizable strategy for reducing phototoxicity and photobleaching.

To explore generalizable strategies for reducing phototoxicity of VF dyes, we were inspired by pioneering work that showed triplet-state quenched, self-healing fluorophores dramatically improve fluorophore performance in single-molecule fluorescence microscopy.[29–33] In this method a triplet-state quencher (TSQ) is tethered to a fluorophore, reducing the lifetime of the triplet state fluorophore through intramolecular triplet energy transfer, decreasing the amount of time that singlet oxygen can be produced, and regenerating the ground state fluorophore in a process called “self-healing.”

To adapt this methodology to voltage imaging, we fused the TSQ cyclooctatetraene (COT) to a fluorescein-based VoltageFluor indicator via a piperazine-cysteic acid linker.[34] VF-COT prolonged imaging time relative to its parent indicator lacking the triplet state quencher. VF-COT also reduced light-induced physiological disruptions in rat hippocampal neurons and hiPSC-CMs like spurious action potentials, runaway firing, or cessation of beating, likely by reducing singlet oxygen and overall ROS production.

Here, we show the self-healing strategy of COT can be used with a silicon-rhodamine based VF dye related to BeRST.[35] **1**-COT is a near-infrared (NIR) BeRST-type VoltageFluor tethered to COT with a piperazine-cysteic acid linker. **1**-COT, like its parent dye, **1**, is voltage sensitive and can report on cardiac action potentials in hiPSC-CMs. In addition, **1**-COT has dramatically improved imaging times in cardiomyocytes compared to **1**, shows reduced phototoxicity, singlet oxygen production, and photobleaching.[35–43]

Results and Discussion

Synthesis.

The synthesis of isoBeRST-pip-cys-COT (**1**-COT) is completed in 2 steps from previously reported compounds. We envisioned a convergent synthesis that first assembled the piperazine-cysteic acid-COT component (**2**) and then coupled it to the Si-rhodamine fluorophore. Synthesis of **2** began by amide coupling of *N*-Boc-piperazine and protected cystine **S1** (**Scheme S1**). Attempts to perform this amide coupling with cysteic acid analogs failed, necessitating the use of the cystine group. Oxidation of the cystine using hydrogen peroxide and formic acid, followed by re-installation of the Boc group provides cysteic acid **S4** in 47% yield over 3 steps. Deprotection of the primary amine followed by an amide coupling with COT-CO_2H yields the cyclooctatetraene amide **2**.

Amide coupling of **2** with Si-rhodamine molecular wire **S0** gave no reaction under multiple conditions (**Scheme S1**), so we instead chose to assemble the COT-conjugated Si-rhodamine fluorophore first and install the molecular wire at a later stage. Deprotection of **2** followed by the coupling with the acid chloride derived from **3** gives silicon rhodamine **S9** in 29% yield (**Scheme S2**). The removal of all of the TFA from the deprotection of **2** was essential for this reaction: trace amounts of TFA decompose the DMF, generating dimethylamine which reacts with the acid chloride of **3** to give a biproduct that was extremely challenging to separate from **S9**. Finally, we developed conditions for the Heck coupling of **S9** with the molecular wire **4**. In the final step, the use of QPhos as a ligand, along with $Pd_2(dba)_3$ as a catalyst, allowed the cross coupling reaction to proceed at 50 °C, rather than the higher temperatures required with $Pd(OAc)_2$/tri-(*o*-tolyl)phosphine, resulting in the isolation of **1**-COT in 41% yield (**Scheme S3**).

In Vitro and Cellular Characterization.

1-COT possesses absorbance and emission spectra characteristic of silicon-rhodamines, with a maximum absorbance at 663 nm and a maximum emission at 683 nm (**Figure 2a**, **Table S1**). These

values are nearly identical to the parent compound **1**.[44] **1**-COT has a quantum yield (Φ_{fl}) of 0.013 (**Table S1**) and localizes to the cell membrane in both HEK293T cells and hiPSC-CMs (**Figure 2b,c**). **1**-COT is voltage sensitive, with a ΔF/F of 11% ± 0.4% per 100 mV (n = 5, S.E.M., **Figure 2d**, **Figure S1**, **Table S1**). The voltage sensitivity of **1**-COT is lower than the sensitivity of **1** (24% ΔF/F).[44] In cells, **1**-COT is 13% as bright as its parent dye, when loaded under identical conditions (**Figure S1c**). The decreased brightness of **1**-COT is likely due, in part, to the lower fluorescence quantum yield of **1**-COT compared to **1** (**Table S1**). In cells, **1**-COT shows improved photostability compared to **1**. After continuous illumination, the fluorescence intensity of **1**-COT in cells remains unchanged at 99.8% of original levels (red trace, **Figure 2e**, n = 18 cells, p = 0.67, two-tailed t-test), while the fluorescence intensity of **1** drops to 90% of its original level (black trace, **Figure 2e**, n = 18 cells, p < 0.0001).

Long Term Recording in Cardiomyocytes.

Both **1** and **1**-COT can visualize cardiac action potentials in hiPSC-CM (**Figure 3**). The ability to optical record action potentials from hiPSC-CMs without disturbing the underlying physiology is a critical requirement for the use of voltage sensitive dyes in sensitive preparations. Compound **1** provides imaging of hiPSC-CM activity under continuous illumination, but only for around 10 minutes. After this time, substantial changes to the underlying cardiac physiology occur. Cardiac action potential duration increases by 38% (**Figure 3**), the beat rate drops by 32% (**Figure S2**), and, most importantly, the cells cease to beat (**Figure 3, Video S1, S2**). On the other hand, **1**-COT enables much longer imaging times. After 30 minutes of imaging with continuous illumination using **1**-COT, hiPSC-CMs continue to beat (**Figure 3**) and show only a modest 19% increase in action potential duration (**Figure 3**, **Video S3-5**). Overall, **1**-COT provides continuous, real-time imaging of hiPSC-CM physiology for 2.7× longer than **1**, pointing to a much lower phototoxicity burden from **1**-COT compared to **1**.

The reduced phototoxicity from **1**-COT may be due to reduced singlet oxygen ($^1O_2$) production which is an effect of the intramolecularly tethered triplet state quencher which promotes self-healing and a reduction of the triplet state of the dye.[32] However since **1**-COT shows reduced relative brightness in cells, the ability of **1**-COT to image for extended periods of time could be related to a smaller effective concentration of indicator loading into the cell membrane. To distinguish between these two possibilities, we compared levels $^1O_2$ production and cellular dye accumulation for both **1** and **1**-COT.

Reduced Singlet Oxygen Production.

We measured production of singlet oxygen resulting from irradiation of **1** and **1**-COT in solution. To do this, we used singlet oxygen sensor green (SOSG), which is highly fluorescent (Φ_{fl} = 0.43) after reaction with singlet oxygen but is weekly fluorescent (Φ_{fl} = 0.009)[43] in the absence of singlet oxygen due to intramolecular PeT quenching fluorescence.[45,46] We monitored the change in fluorescence of SOSG (ΔF/F) in samples containing SOSG and **1**, **1**-COT, or buffer (**Figure 4a**).

1-COT produces lower amounts of $^1O_2$ than **1**. Irradiation of **1**-COT at 631 nm for 10 min in the presence of SOSG results in a 7% increase in SOSG fluorescence over background (**Figure 4a**, red, ±4.3%, S.E.M., n = 4), which is not a significant difference (p = 0.51, Tukey's post-hoc comparison, **Figure 4a**). On the other hand, **1** produces nearly 5× more $^1O_2$ than **1**-COT. Irradiation of **1** in the presence of SOSG results in a 33% increase in SOSG fluorescence (**Figure 4a**, black, ±3.3%, S.E.M., n = 4), which is a statistically significant difference (p < 0.001, Tukey's post-hoc comparison, **Figure 4a**). Together, these results show that 1-COT produces lower amounts of $^1O_2$ compared to **1**, consistent with the proposed mechanism of self-healing fluorophores.[29,32] The decreased rate of $^1O_2$ production by **1**-COT likely contributes to the improved photostability in HEK cells (**Figure 2e**) and reduced phototoxicity in hiPSC-CMs (**Figure 3a**).

Reduced loading of 1-COT.

1-COT boasts the ability to image cardiac electrophysiology for about three times longer than **1**. The reduced toxicity of **1**-COT is due, in part, to the decreased production of $^1O_2$, as established above. However, reduced phototoxicity could also be a result of decreased accumulation of **1**-COT in the

plasma membrane of cells, even when applied at the same concentration as **1**. The cellular brightness of **1**-COT is about 7× less than the parent dye (**Figure S1**). The lower brightness of **1**-COT in cells is partly due to its lower intrinsic brightness of 1.2 ($\Phi_{fl} \times \varepsilon$, **Table S1**), which is about 7× lower than the brightness of **1** ($\Phi_{fl} \times \varepsilon = 8.6$, **Table S1**).

To confirm this, we performed fluorescence lifetime imaging microscopy (FLIM) on HEK cells loaded with either **1** or **1**-COT, to determine an estimate of the "in situ" fluorescence quantum yield in a plasma membrane (since fluorescence lifetime, or τ_{fl}, is inversely proportional to the fluorescence quantum yield). In HEK cells, **1** (200 nM) has a fluorescence lifetime of approximately 0.83 ns (± 0.02 ns, S.E.M., n = 9), while **1**-COT has a τ_{fl} of approximately 1.46 ns (±0.03, S.E.M., n = 8). The longer lifetime of **1**-COT in the plasma membrane is not consistent with the *in vitro* fluorescence quantum yields. This discrepancy suggests two things: first, that **1**-COT is a brighter fluorophore than **1** in cell membranes, and second, that *in vitro* conditions for determining fluorescence quantum yields are not a good mimic for the plasma bilayer.

If **1**-COT has a higher fluorescence quantum yield than **1** in the plasma membrane, what accounts for the decreased overall brightness? It could be that less **1**-COT is loading in the membrane than **1**. To test this, we looked at the concentration dependence of the fluorescence lifetime in HEK cells. We previously showed that, at high dye loading concentrations, plasma membrane dyes show a decrease in fluorescence lifetime.[47–49]A greater concentration dependence on the τ_{fl} indicates a higher degree of membrane loading. The τ_{fl} of **1** shows greater dependence on dye concentration than **1**-COT (**Figure 4b/c**). For **1**-COT, τ_{fl} values at different concentrations range from 1.43 ns to 1.53 ns, and there is no significant difference between the lifetimes at any concentration ranging from 200 nM to 1 μM (**Figure 4b**, $p > 0.05$, ANOVA). Whereas for **1**, fluorescence lifetime at concentrations of 500 nM and above are significantly lower than the τ_{fl} at 200 nM (**Figure 4c**, $p < 0.005$, ANOVA + Tukey's post-hoc analysis of multiple comparisons). These data suggest that **1** loads more effectively into membranes than **1**-COT. So, while **1**, with its lower τ_{fl} in cell membranes, is intrinsically dimmer than **1**-COT, there is more of **1** in the membrane, making the fluorescence intensity greater.

Conclusion

In this study, we show that **1**-COT is a voltage sensitive fluorophore with improved photostability and reduced toxicity in cardiomyocytes. Compared to the unmodified dye, **1**-COT is less bright in cells and shows decreased voltage sensitivity. The reduced toxicity of **1**-COT, which enables a nearly 3× increase in imaging time in cardiomyocytes, is due in part to decreased production of $^1O_2$, which is consistent with the mechanism of triplet state quenching in self-healing fluorophores.[50] The reduced toxicity of **1**-COT may also come from a lower effective concentration in the plasma membrane, since FLIM experiments reveal very little concentration-dependence of the τ_{fl} for **1**-COT.

Despite the dramatic increase in imaging time in cardiomyocytes, real challenges remain that limit the current utility of **1**-COT and guide future directions for research. First, unlike fluorescein-based COT-stabilized dyes, in which the COT-functionalized dye has the same voltage sensitivity as the unmodified dye, the voltage sensitivity of **1**-COT is lower than that of **1**. Additionally, the lower cellular brightness of **1**-COT compared to **1** substantially limits application of **1**-COT. The low cellular brightness of **1**-COT may come from its poor solubility. The use of COT as a TSQ via an amide linkage removes a positive charge from **1**, which may contribute to the overall lower solubility and poor membrane loading. The addition of the COT group may also change the orientation of **1**-COT in the membrane, which would decrease its voltage sensitivity.[51] Future directions for improving the performance of TSQ-stabilized Si-rhodamine dyes include improving solubility and the exploration of less hydrophobic triplet state quenchers.

Acknowledgments

We acknowledge support from NIH (R35GM119855) and DOE (DE-SC0023184). NCG was supported by an NIH NRSA Fellowship (F32GM139263). KNM was supported, in part, by a training grant from the NIH (T32GM066698).

Figures and Schemes

Figure 1. Structure of **1**-COT and **1**.

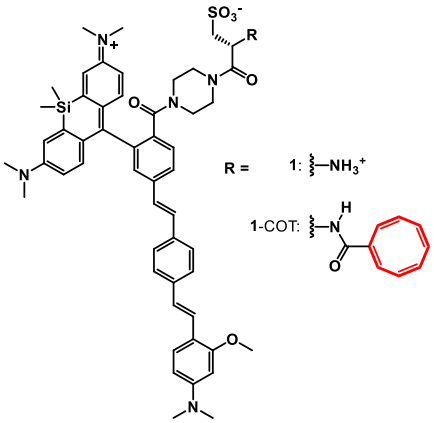

Structures of Voltage Fluor (VF) dyes based on Si-rhodamine BeRST.

Scheme 1. Synthesis of **1**-COT.

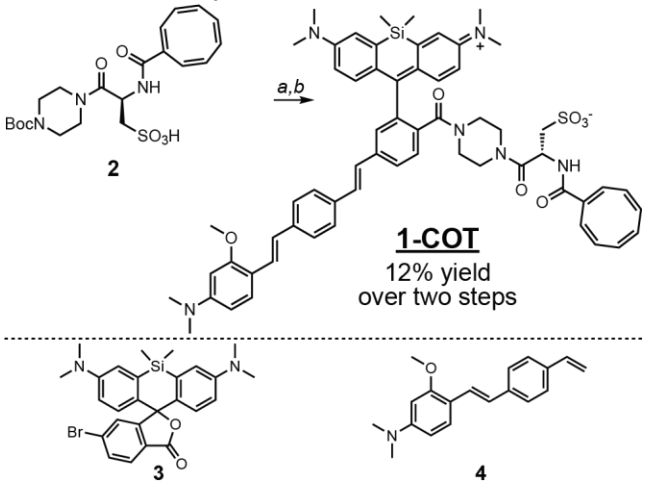

Conditions: **a)** i) TFA, CH_2Cl_2, rt, ii) **3**, $(COCl)_2$, CH_2Cl_2, rt, iii) Et_3N, DMF, rt; **b)** **4**, cat. Pd_2dba_3, QPhos, Et_3N, DMF, 50 °C.

Figure 2. Characterization of **1**-COT.

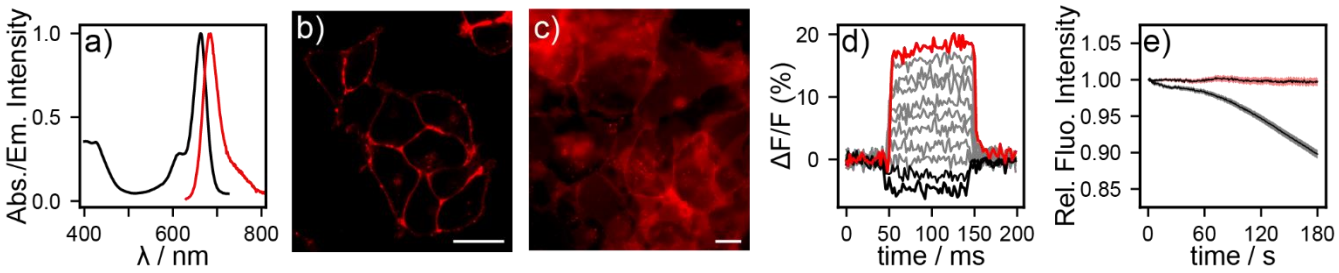

a) Absorbance (black) and emission (red) profile of **1**-COT. Fluorescence images of **1**-COT loaded at 0.5 μM in **b)** HEK293T cells (confocal) and **c)** hiPSC-CMs (epifluorescence). Scale bars are 20 μm. **d)** Plot of relative change in fluorescence of **1**-COT (ΔF/F) vs. time in a patch-clamped HEK293T cell under whole-cell voltage-clamp conditions. **e)** Plot of relative fluorescence intensity vs time for **1** (black) or **1**-COT (red) in HEK293T cells. Shaded area represents the standard error of the mean for n = 18 individual cell rafts.

Figure 3. Characterization of action potential parameters.

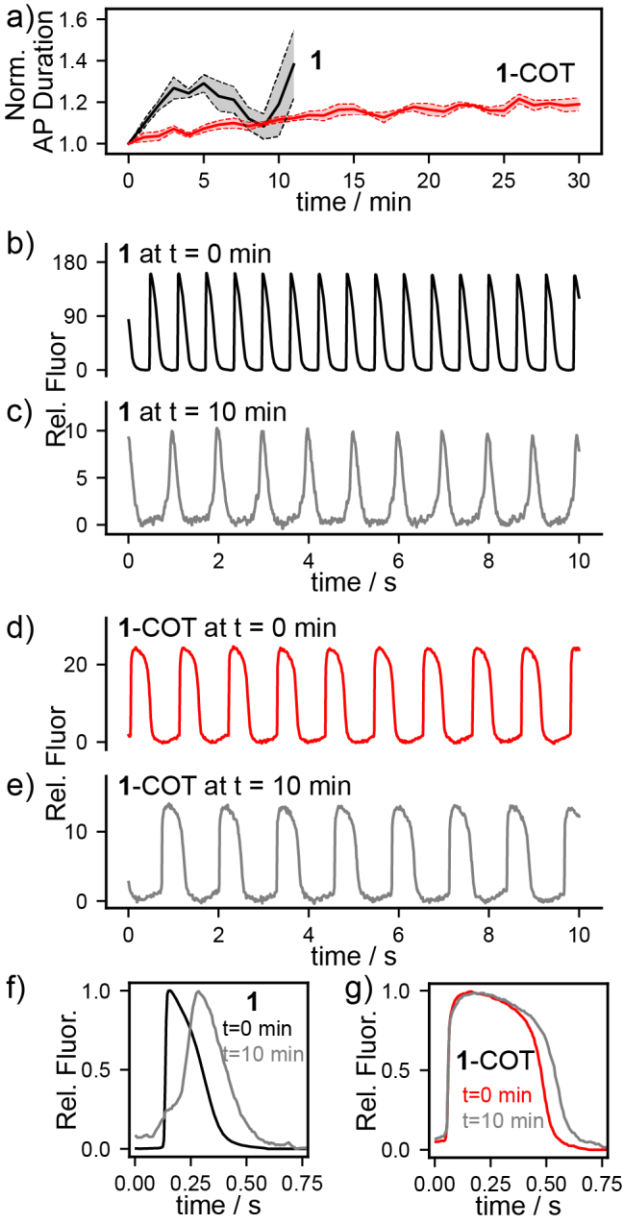

a) Plot of normalized action potential duration over time for **1** (black) and **1**-COT (red). At every minute, a 10 s acquisition was taken, and the action potential duration was measured. Data are a mean ± SEM of n = 3 trials. Plots of fluorescence intensity versus time demonstrating a representative action potential trace during a phototoxicity assay for **b) 1** at t = 0 min, **c) 1** at t = 10 min, **d) 1**-COT at t = 0 min, and **e) 1**-COT at t = 10 min. Average action potentials as optically recorded at t = 0 min and t = 10 min using **f) 1** (black/grey) and **g) 1**-COT (red/grey). Average traces are representative of the overall action potential traces shown in figure 3b-e.

Figure 4. 1-COT produces less $^1O_2$ than **1** and shows poor plasma membrane accumulation.

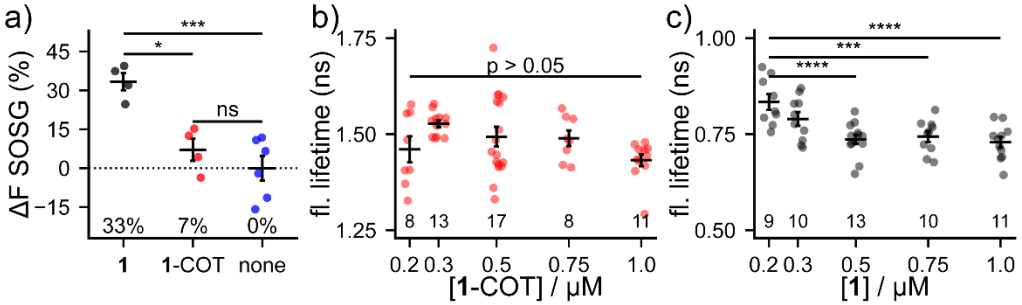

a) Relative changes in SOSG emission in solution after continuous illumination of samples for 10 minutes. Concentrations for all dyes are 1 μM. Solutions represented are: **1** with SOSG present (grey); **1**-COT with SOSG present (red); and SOSG in solution (blue). ANOVA test with Tukey's post-hoc analysis for multiple comparisons (*: $p < 0.01$; ***: $p < 0.001$; ns: $p = 0.51$). Plot of fluorescence lifetime vs. dye concentration for **b) 1**-COT and **c) 1**. Each point represents a group of cells; the total number of groups analyzed is listed for each condition. For **1**-COT, there were no significant differences between groups (ANOVA, $p > 0.05$). For **1**-COT, there were significant differences between the groups (ANOVA); Tukey's post-hoc analysis comparisons between group revealed significant differences (**: $p < 0.005$; ****: $p < 0.0005$).

References

(1) Garg, P.; Garg, V.; Shrestha, R.; Sanguinetti, M. C.; Kamp, T. J.; Wu, J. C. Human Induced Pluripotent Stem Cell-Derived Cardiomyocytes as Models for Cardiac Channelopathies: A Primer for Non-Electrophysiologists. *Circ. Res.* **2018**, *123* (2), 224–243. https://doi.org/10.1161/CIRCRESAHA.118.311209.

(2) Acker, C. D.; Yan, P.; Loew, L. M. Recent Progress in Optical Voltage-Sensor Technology and Applications to Cardiac Research : From Single Cells to Whole Hearts. *Prog. Biophys. Mol. Biol.* **2019**, No. xxxx. https://doi.org/10.1016/j.pbiomolbio.2019.07.004.

(3) Berenfeld, O.; Mandapati, R.; Dixit, S.; Skanes, A. C.; Chen, J.; Mansour, M.; Jalife, J. Spatially Distributed Dominant Excitation Frequencies Reveal Hidden Organization in Atrial Fibrillation in the Langendorff-Perfused Sheep Heart. *J. Cardiovasc. Electrophysiol.* **2000**, *11* (8), 869–879. https://doi.org/10.1111/j.1540-8167.2000.tb00066.x.

(4) Mironov, S.; Jalife, J.; Tolkacheva, E. G. Role of Conduction Velocity Restitution and Short-Term Memory in the Development of Action Potential Duration Alternans in Isolated Rabbit Hearts. *Circulation* **2008**, *118* (1), 17–25. https://doi.org/10.1161/CIRCULATIONAHA.107.737254.

(5) Herron, T. J. Calcium and Voltage Mapping in HiPSC-CM Monolayers. *Cell Calcium* **2016**, *59* (2–3), 84–90. https://doi.org/10.1016/j.ceca.2016.02.004.

(6) Huebsch, N.; Charrez, B.; Neiman, G.; Siemons, B.; Boggess, S. C.; Wall, S.; Charwat, V.; Jæger, K. H.; Cleres, D.; Telle, Å.; Lee-Montiel, F. T.; Jeffreys, N. C.; Deveshwar, N.; Edwards, A. G.; Serrano, J.; Snuderl, M.; Stahl, A.; Tveito, A.; Miller, E. W.; Healy, K. E. Metabolically Driven Maturation of Human-Induced-Pluripotent-Stem-Cell-Derived Cardiac Microtissues on Microfluidic Chips. *Nat. Biomed. Eng.* **2022**, *6* (4), 372–388. https://doi.org/10.1038/s41551-022-00884-4.

(7) McNamara, H. M.; Dodson, S.; Huang, Y. L.; Miller, E. W.; Sandstede, B.; Cohen, A. E. Geometry-Dependent Arrhythmias in Electrically Excitable Tissues. *Cell Syst.* **2018**, *7* (4), 359-370.e6. https://doi.org/10.1016/j.cels.2018.08.013.

(8) Muñoz, J. J. A. M.; Dariolli, R.; da Silva, C. M.; Neri, E. A.; Valadão, I. C.; Turaça, L. T.; Lima, V. M.; de Carvalho, M. L. P.; Velho, M. R.; Sobie, E. A.; Krieger, J. E. Time-Regulated Transcripts with the Potential to Modulate Human Pluripotent Stem Cell-Derived Cardiomyocyte Differentiation. *Stem Cell Res. Ther.* **2022**, *13* (1), 1–27. https://doi.org/10.1186/s13287-022-03138-x.

(9) Narkar, A.; Willard, J. M.; Blinova, K. Chronic Cardiotoxicity Assays Using Human Induced Pluripotent Stem Cell-Derived Cardiomyocytes (HiPSC-CMs). *Int. J. Mol. Sci.* **2022**, *23* (6). https://doi.org/10.3390/ijms23063199.

(10) Charrez, B.; Charwat, V.; Siemons, B. A.; Goswami, I.; Sakolish, C.; Luo, Y. S.; Finsberg, H.; Edwards, A. G.; Miller, E. W.; Rusyn, I.; Healy, K. E. Heart Muscle Microphysiological System for Cardiac Liability Prediction of Repurposed COVID-19 Therapeutics. *Front. Pharmacol.* **2021**, *12* (August), 1–15. https://doi.org/10.3389/fphar.2021.684252.

(11) Charwat, V.; Charrez, B.; Siemons, B. A.; Finsberg, H.; Jæger, K. H.; Edwards, A. G.; Huebsch, N.; Wall, S.; Miller, E.; Tveito, A.; Healy, K. E. Validating the Arrhythmogenic Potential of High-, Intermediate-, and Low-Risk Drugs in a Human-Induced Pluripotent Stem Cell-Derived Cardiac Microphysiological System. *ACS Pharmacol. Transl. Sci.* **2022**, *5* (8), 652–667. https://doi.org/10.1021/acsptsci.2c00088.

(12) Arslanova, A.; Shafaattalab, S.; Lin, E.; Barszczewski, T.; Hove-Madsen, L.; Tibbits, G. F. Investigating Inherited Arrhythmias Using HiPSC-Derived Cardiomyocytes. *Methods* **2022**, *203* (June 2021), 542–557. https://doi.org/10.1016/j.ymeth.2021.06.015.

(13) Salama, G.; Morad, M. Merocyanine 540 as an Optical Probe of Transmembrane Electrical Activity in the Heart. *Science (80-.).* **1976**, *191* (4226), 485–487.

https://doi.org/10.1126/science.191.4226.485.

(14) Herron, T. J.; Lee, P.; Jalife, J. Optical Imaging of Voltage and Calcium in Cardiac Cells & Tissues. *Circ. Res.* **2012**, *110* (4), 609–623. https://doi.org/10.1161/CIRCRESAHA.111.247494.Optical.

(15) Efimov, I. R.; Nikolski, V. P.; Salama, G. Optical Imaging of the Heart. *Circ. Res.* **2004**, *95* (1), 21–33. https://doi.org/10.1161/01.RES.0000130529.18016.35.

(16) Loew, L. M.; Scully, S.; Simpson, L.; Waggoner, A. S. Evidence for a Charge-Shift Electrochromic Mechanism in a Probe of Membrane Potential. *Nature* **1979**, *281* (5731), 497–499. https://doi.org/10.1038/281497a0.

(17) Schaffer, P.; Ahammer, H.; Müller, W.; Koidl, B.; Windisch, H. Di-4-ANEPPS Causes Photodynamic Damage to Isolated Cardiomyocytes. *Pflügers Arch. Eur. J. Physiol.* **1994**, *426* (6), 548–551. https://doi.org/10.1007/BF00378533.

(18) Fluhler, E.; Burnham, V. G.; Loew, L. M. Spectra, Membrane Binding, and Potentiometric Reponses of New Charge Shift Probes†. *Biochemistry* **1985**, *24* (21), 5749–5755. https://doi.org/10.1021/bi00342a010.

(19) Icha, J.; Weber, M.; Waters, J. C.; Norden, C. Phototoxicity in Live Fluorescence Microscopy, and How to Avoid It. *BioEssays* **2017**, *39* (8), 1–15. https://doi.org/10.1002/bies.201700003.

(20) Tinevez, J. Y.; Dragavon, J.; Baba-Aissa, L.; Roux, P.; Perret, E.; Canivet, A.; Galy, V.; Shorte, S. *A Quantitative Method for Measuring Phototoxicity of a Live Cell Imaging Microscope*, 1st ed.; Elsevier Inc., 2012; Vol. 506. https://doi.org/10.1016/B978-0-12-391856-7.00039-1.

(21) Skylaki, S.; Hilsenbeck, O.; Schroeder, T. Challenges in Long-Term Imaging and Quantification of Single-Cell Dynamics. *Nat. Biotechnol.* **2016**, *34* (11), 1137–1144. https://doi.org/10.1038/nbt.3713.

(22) Rohr, S.; Salzberg, B. Multiple Site Optical Recording of Transmembrane Voltage (MSORTV) in Patterned Growth Heart Cell Cultures: Assessing Electrical Behavior, with Microsecond Resolution, on a Cellular and Subcellular Scale. *Biophys. J.* **1994**, *67* (3), 1301–1315. https://doi.org/10.1016/S0006-3495(94)80602-2.

(23) Miller, E. W.; Lin, J. Y.; Frady, E. P.; Steinbach, P. a; Kristan, W. B.; Tsien, R. Y. Optically Monitoring Voltage in Neurons by Photo-Induced Electron Transfer through Molecular Wires. *Proc. Natl. Acad. Sci. U. S. A.* **2012**, *109* (6), 2114–2119. https://doi.org/10.1073/pnas.1120694109.

(24) Li, L. S. Fluorescence Probes for Membrane Potentials Based on Mesoscopic Electron Transfer. *Nano Lett.* **2007**, *7* (10), 2981–2986. https://doi.org/10.1021/nl071163p.

(25) de Silva, A. P.; Gunaratne, H. Q. N.; Habib-Jiwan, J. -L; McCoy, C. P.; Rice, T. E.; Soumillion, J. -P. New Fluorescent Model Compounds for the Study of Photoinduced Electron Transfer: The Influence of a Molecular Electric Field in the Excited State. *Angew. Chemie Int. Ed. English* **1995**, *34* (16), 1728–1731. https://doi.org/10.1002/anie.199517281.

(26) Liu, P.; Miller, E. W. Electrophysiology, Unplugged: Imaging Membrane Potential with Fluorescent Indicators. *Acc. Chem. Res.* **2020**, *53* (1), 11–19. https://doi.org/10.1021/acs.accounts.9b00514.

(27) Boggess, S. C.; Gandhi, S. S.; Siemons, B. A.; Huebsch, N.; Healy, K. E.; Miller, E. W. New Molecular Scaffolds for Fluorescent Voltage Indicators. *ACS Chem. Biol.* **2019**, *14* (3), 390–396. https://doi.org/10.1021/acschembio.8b00978.

(28) Boggess, S.; Gandhi, S.; Benlian, B.; Miller, E. Vinyl-Fluorene Molecular Wires for Voltage Imaging with Enhanced Sensitivity and Reduced Phototoxicity. *J. Am. Chem. Soc. 143* (31), 11903–11907. https://doi.org/10.1021/jacs.1c04543.

(29) Zheng, Q.; Jockusch, S.; Zhou, Z.; Altman, R. B.; Zhao, H.; Asher, W.; Holsey, M.; Mathiasen, S.; Geggier, P.; Javitch, J. A.; Blanchard, S. C. Electronic Tuning of Self-Healing Fluorophores for Live-Cell and Single-Molecule Imaging. *Chem. Sci.* **2016**, *8* (1), 755–762. https://doi.org/10.1039/C6SC02976K.

(30) Yang, Z.; Li, L.; Ling, J.; Liu, T.; Huang, X.; Ying, Y.; Zhao, Y.; Zhao, Y.; Lei, K.; Chen, L.; Chen, Z. Cyclooctatetraene-Conjugated Cyanine Mitochondrial Probes Minimize Phototoxicity in Fluorescence and Nanoscopic Imaging. *Chem. Sci.* **2020**, *11* (32), 8506–8516. https://doi.org/10.1039/d0sc02837a.

(31) Zheng, Q.; Jockusch, S.; Zhou, Z.; Blanchard, S. C. The Contribution of Reactive Oxygen Species to the Photobleaching of Organic Fluorophores. *Photochem. Photobiol.* **2014**, *90* (2), 448–454. https://doi.org/10.1111/php.12204.

(32) Zheng, Q.; Jockusch, S.; Zhou, Z.; Altman, R. B.; Warren, J. D.; Turro, N. J.; Blanchard, S. C. On the Mechanisms of Cyanine Fluorophore Photostabilization. *J. Phys. Chem. Lett.* **2012**, *3* (16), 2200–2203. https://doi.org/10.1021/jz300670p.

(33) Frutos, L. M.; Castaño, O.; Andrés, J. L.; Merchán, M.; Acuña, A. U. A Theory of Nonvertical Triplet Energy Transfer in Terms of Accurate Potential Energy Surfaces: The Transfer Reaction from π, Π* Triplet Donors to 1,3,5,7-Cyclooctatetraene. *J. Chem. Phys.* **2004**, *120* (3), 1208–1216. https://doi.org/10.1063/1.1631418.

(34) Grenier, V.; Martinez, K.; Benlian, B.; García-Almedina, D.; Raliski, B.; Boggess, S.; Maza, J.; Yang, S.; Gest, A.; Miller, E. Molecular Prosthetics for Long-Term Functional Imaging with Fluorescent Reporters. *ACS Cent. Sci.* *8* (1), 118–121. https://doi.org/10.1021/acscentsci.1c01153.

(35) Huang, Y. L.; Walker, A. S.; Miller, E. W. A Photostable Silicon Rhodamine Platform for Optical Voltage Sensing. *J. Am. Chem. Soc.* **2015**, *137* (33), 10767–10776. https://doi.org/10.1021/jacs.5b06644.

(36) McNamara, H. M.; Salegame, R.; Tanoury, Z. Al; Xu, H.; Begum, S.; Ortiz, G.; Pourquie, O.; Cohen, A. E. Bioelectrical Domain Walls in Homogeneous Tissues. *Nat. Phys.* **2020**, *16* (3), 357–364. https://doi.org/10.1038/s41567-019-0765-4.

(37) Tveito, A.; Jæger, K. H.; Huebsch, N.; Charrez, B.; Edwards, A. G.; Wall, S.; Healy, K. E. Inversion and Computational Maturation of Drug Response Using Human Stem Cell Derived Cardiomyocytes in Microphysiological Systems. *Sci. Rep.* **2018**, *8* (1), 1–14. https://doi.org/10.1038/s41598-018-35858-7.

(38) Jæger, K. H.; Charwat, V.; Charrez, B.; Finsberg, H.; Maleckar, M. M.; Wall, S.; Healy, K. E.; Tveito, A. Improved Computational Identification of Drug Response Using Optical Measurements of Human Stem Cell Derived Cardiomyocytes in Microphysiological Systems. *Front. Pharmacol.* **2020**, *10* (February), 1–24. https://doi.org/10.3389/fphar.2019.01648.

(39) Huebsch, N.; Charrez, B.; Siemons, B.; Boggess, S. C.; Wall, S.; Charwat, V.; Jæger, K. H.; Cleres, D.; Telle, Å.; Lee-montiel, F. T.; Jeffreys, N. C.; Deveshwar, N.; Edwards, A.; Serrano, J.; Snuderl, M. Metabolically-Driven Maturation of HiPSC-Cell Derived Cardiac Chip. *bioRxiv* **2020**, No. 510.

(40) Lee-Montiel, F.; Laemmle, A.; Dumont, L.; Lee, C.; Huebsch, N.; Charwat, V.; Okochi, H.; Hancock, M.; Siemons, B.; Boggess, S.; Goswami, I.; Miller, E.; Willenbring, H.; Healy, K. Integrated HiPSC-Based Liver and Heart Microphysiological Systems Predict Unsafe Drug-Drug Interaction. *bioRxiv* **2020**. https://doi.org/10.1101/2020.05.24.112771.

(41) Charrez, B.; Charwat, V.; Siemons, B.; Finsberg, H.; Miller, E.; Edwards, A. G.; Healy, K. E. In Vitro Safety “Clinical Trial” of the Cardiac Liability of Hydroxychloroquine and Azithromycin as COVID19 Polytherapy. *bioRxiv* **2020**, *10090*. https://doi.org/10.1101/2020.12.21.423869.

(42) Klimas, A.; Ortiz, G.; Boggess, S. C.; Miller, E. W.; Entcheva, E. Multimodal On-Axis Platform for

All-Optical Electrophysiology with near-Infrared Probes in Human Stem-Cell-Derived Cardiomyocytes. *Prog. Biophys. Mol. Biol.* **2019**, *3* (xxxx), 1–9. https://doi.org/10.1016/j.pbiomolbio.2019.02.004.

(43) Boggess, S.; Gandhi, S.; Siemons, B.; Huebsch, N.; Healy, K.; Miller, E.; Boggess, C.; New, E.; Scaffolds, M.; Indicators, V.; Preprint, C.; Boggess, S. C.; Gandhi, S. S.; Siemons, B. A.; Huebsch, N.; Healy, K. E.; Miller, E. W. New Molecular Scaffolds for Fluorescent Voltage Indicators New Molecular Scaffolds for Fluorescent Voltage Indicators. **2018**, No. 2. https://doi.org/10.26434/chemrxiv.7338683.v1.

(44) Ortiz, G.; Liu, P.; Deal, P. E.; Nensel, A. K.; Martinez, K. N.; Shamardani, K.; Adesnik, H.; Miller, E. W. A Silicon-Rhodamine Chemical-Genetic Hybrid for Far Red Voltage Imaging from Defined Neurons in Brain Slice. *RSC Chem. Biol.* **2021**, *2* (6), 1594–1599. https://doi.org/10.1039/d1cb00156f.

(45) Gollmer, A.; Arnbjerg, J.; Blaikie, F. H.; Pedersen, B. W.; Breitenbach, T.; Daasbjerg, K.; Glasius, M.; Ogilby, P. R. Singlet Oxygen Sensor Green®: Photochemical Behavior in Solution and in a Mammalian Cell. *Photochem. Photobiol.* **2011**, *87* (3), 671–679. https://doi.org/10.1111/j.1751-1097.2011.00900.x.

(46) Kim, S.; Fujitsuka, M.; Majima, T. Photochemistry of Singlet Oxygen Sensor Green. *J. Phys. Chem. B* **2013**, *117* (45), 13985–13992. https://doi.org/10.1021/jp406638g.

(47) Chen, W.; Young, L. J.; Lu, M.; Zaccone, A.; Strohl, F.; Yu, N.; Schierle, G. S. K.; Kaminski, C. F. Fluorescence Self-Quenching from Reporter Dyes Informs on the Structural Properties of Amyloid Clusters Formed in Vitro and in Cells. *Nano Lett.* **2017**, *17* (1), 143–149. https://doi.org/10.1021/acs.nanolett.6b03686.

(48) Chen, R. F.; Knutson, J. R. Mechanism of Fluorescence Concentration Quenching of Carboxyfluorescein in Liposomes: Energy Transfer to Nonfluorescent Dimers. *Anal. Biochem.* **1988**, *172* (1), 61–77. https://doi.org/10.1016/0003-2697(88)90412-5.

(49) Boggess, S. C.; Lazzari-Dean, J. R.; Raliski, B. K.; Mun, D. M.; Li, A. Y.; Turnbull, J. L.; Miller, E. W. Fluorescence Lifetime Predicts Performance of Voltage Sensitive Fluorophores in Cardiomyocytes and Neurons. *RSC Chem. Biol.* **2021**. https://doi.org/10.1039/d0cb00152j.

(50) Berezin, M. Y.; Achilefu, S. Fluorescence Lifetime Measurements and Biological Imaging. *Chem. Rev.* **2010**, *110* (5), 2641–2684. https://doi.org/10.1021/cr900343z.

(51) Kulkarni, R.; Adil, M.; Yin, H.; Pourmandi, N.; James, F.; Schaffer, D.; Wang, Y.; Miller, E. A Rationally Designed, General Strategy for Membrane Orientation of Photoinduced Electron Transfer-Based Voltage-Sensitive Dyes. *ACS Chem. Biol. 12* (2), 407–413. https://doi.org/10.1021/acschembio.6b00981.